Seismicity and noise recorded by passive seismic monitoring of drilling operations offshore the eastern Canary Islands

Arantza Ugalde[1,2], Beatriz Gaite[1,3], Mario Ruiz[1], Antonio Villaseñor[1], César R. Ranero[2]

[1] Institute of Earth Sciences Jaume Almera - CSIC, Lluís Solé i Sabarís, s/n, 08028 Barcelona, Spain. E-mail: mruiz@ictja.csic.es; antonio@ictja.csic.es

[2] Now at: Institute of Marine Sciences - CSIC, Pg. Marítim de la Barceloneta 37- 49, 08003 Barcelona, Spain. E-mail: a.ugalde@icm.csic.es; cranero@cmima.csic.es

[3] Now at: Instituto Geográfico Nacional, c. General Ibáñez de Ibero, 3, 28003 Madrid, Spain. E-mail: bgaite@fomento.es

Arantza Ugalde, Beatriz Gaite, Mario Ruiz, Antonio Villaseñor, César R. Ranero; Seismicity and Noise Recorded by Passive Seismic Monitoring of Drilling Operations Offshore the Eastern Canary Islands. Seismological Research Letters ; 90 (4): 1565–1576. doi: https://doi.org/10.1785/0220180353

ABSTRACT

In November 2014 a temporary land and marine seismic network was deployed to monitor the drilling of an exploratory well in the Canary Channel (Eastern Canary Islands). This region is characterized by low seismic activity; however, because of the increased awareness of the potential seismic hazard caused by hydrocarbon exploitation activities, the drilling operations were monitored with an unprecedented level of detail for an activity of this kind. According to the reported earthquakes, there was not a measurable increase in seismicity in the vicinity of the well. Overall seismic activity was low, which is consistent with the historical seismicity records. Harmonic tremor, explained here as resonances of the instrument-seafloor system generated by bottom water currents in the area, was commonly detected on the ocean bottom seismometer (OBS) recordings. The marine network data also revealed few dozens of non-seismic short-duration signals per day that appear similar to other events on OBS recorded throughout the world. We suggest that they may be caused by direct perturbations on the OBS, mostly induced by ocean currents in the Canary Channel.

INTRODUCTION

A broad range of industrial activities, such as oil and gas injection and extraction, geothermal projects, hydraulic fracturing, waste fluid disposal, water reservoir impoundment, and mining, can be the source of human-induced seismicity (e.g., Wilson *et al.*, 2017; Foulger *et al.*, 2018). Earthquakes are induced by perturbations in the mechanical state of the rocks through various physical mechanisms (e.g., Eaton, 2018). The evaluation of the general seismicity patterns in a region through seismic activity monitoring may reveal areas where unusual seismic activity can be correlated in space and time to industrial activities (e.g., National Research Council, 2013).

From November 2014 to January 2015, RIPSA (Repsol Investigaciones Petrolíferas SA) carried out an exploratory drilling survey 3,500 meters below the sea level in the Canary Channel, at about 50 km offshore the easternmost islands of the Canary archipelago (Figure 1). Although seismicity may increase in hydrocarbon reservoirs due to industrial activities, examples of earthquakes triggered by hydrocarbon exploratory drilling are not documented to our knowledge. Nevertheless, in light of the environmental impact assessment report, the Spanish Directorate General of Energy Policy and Mines required passive seismic monitoring of the hydrocarbon drilling activities in the area as a precautionary approach (BOE, 2014). The real time seismic monitoring was used to operate a risk management system through a traffic-light warning protocol that set out the thresholds (green, yellow and red light levels) for taking mitigation actions in response to the detection of uncommon levels of seismic activity. Under the traffic-light scheme implemented, the drilling operations should be halted if a seismic event with magnitude greater than 4.5 was detected at a distance less than 75 km from the exploration well. The protocol allowed further steps to be taken if an event with a magnitude less than 4.5 or an earthquake swarm occurred within a radius of 20 km from the drilling site.

The region east of Lanzarote and Fuerteventura islands is characterized by low seismic activity (e.g., González de Vallejo *et al.*, 2006); however, moderate earthquakes have occurred in this area in recent years, some of them being felt by the population, such as the 6 September 2003 (m_b 4.5) event SE of Lanzarote (EMS intensity III-IV). Moreover, the 11 June 2013 (m_b 3.7) earthquake that was felt with EMS intensity II in Lanzarote occurred close to the drilling location. Seismic activity in the region is continuously monitored by the IGN (Instituto Geográfico Nacional, network code ES). Nevertheless, the azimuthal gap of the permanent seismic network geometry in the area of interest is high, and the nearest station is located more than 50 km to the west of the drilling site (Figure 1). To provide a baseline against which any variation of seismic activity could be detected, we deployed a temporary seismic network formed by 21 land stations in the Canary Islands and southwestern Morocco and 17 ocean bottom seismometers (OBS) in the vicinity of the well. The OBS network was deployed for 20 days prior to, for the full duration of, and for 1 month after the exploratory drilling, that took place from November 18, 2014 to January 11, 2015. The land stations operated from 2 months before, to 9 months after the drilling operations.

In this work we present the seismic monitoring network performance in the eastern Canary Islands, including the background noise levels and the seismicity rates observed for the 12 months of seismic monitoring. We also examine other high-frequency non-seismic signals recorded by the OBS network during its full 3-month period of monitoring.

GEOLOGICAL SETTING

The Canary Channel extends between the SSW-NNE volcanic ridge of Fuerteventura-Lanzarote (the Canary Ridge) and the Western Africa passive continental margin. It resulted from the elevation of the Canary Ridge since the Oligocene by volcanism. Fuerteventura and Lanzarote Islands are built on the upper continental rise, at a water depth of about 2,000 m and at a distance of 100 km from the African coast. They are in the post-erosional stage of volcanic activity (Carracedo, 1999). The crust in the easternmost islands of the Canary archipelago is 11-15 km thick (Banda *et al.*, 1981). This area is located at the transition between continental and oceanic crust and is characterized by a 10-km-thick sediment layer east of the ridge (e.g., Rivera *et al.*, 2016). The central seafloor surface of the Canary Channel extends between 1,240 m and 1,460 m water depth, and its most significant features are submarine hills of volcanic or diapiric origin (Acosta *et al.*, 2005). Along the Canary Channel, early Triassic evaporitic diapirs intrude Mesozoic sedimentary units and form mounds when they reach the seabed (Rivera *et al.*, 2016). The diapir belt has gained the interest of oil companies for hydrocarbon exploration and it was the focus of the drilling activities monitored in this work.

SEISMIC NETWORK CONFIGURATION

The temporary land network consisted of 8 broadband seismic stations in the Eastern Canary Islands (4 in Lanzarote and 4 in Fuerteventura) and 11 stations in southwestern Morocco (Figure 1). All the stations were equipped with a Nanometrics Trillium 120P broadband seismometer and a Taurus digitizer. The instruments had a flat velocity response between 120 s and 40 Hz. Data were continuously recorded on-site with a sampling rate of 100 samples per second (sps). The stations in Morocco were configured to sample data at 50 sps. Data were also transmitted to the ICTJA-CSIC via GPRS using the real-time protocol Seedlink. The network included 2 additional stations at Arrecife (Lanzarote) and Puerto del Rosario (Fuerteventura) capital cities, each with a Sara SA10 force balance accelerometer and a Worldsensing Spidernano digitizer. The accelerometric stations were part of the seismic warning protocol and could be interrogated after an earthquake via GPRS communication links.

The marine network was composed of 17 LC SP 4x4 OBSs designed by the Scripps Institution of Oceanography, each with three-component, Sercel L-28 4.5 Hz geophones and a HighTech HTI-90-U hydrophone. The instruments were set to continuous recording of data with a sampling rate of 100 sps. The OBSs were deployed around the drilling hole at depths between 709 m and 1,355 m with interstation distances from about 5 km to 17 km (Figure 1). The actual orientations of the horizontal components of the geophones are not determined and they are referred to as channels EH1 and EH2.

GENERAL AMBIENT NOISE LEVELS

To assess the typical seismic ambient noise levels at each site of the temporary network, we analyzed the data spectral characteristics using the software PQLX (McNamara and Boaz, 2011). This package computes the power spectral densities (PSD) for all the available data from 1-hour length, continuous, instrument corrected, 50% overlapping time segments following the procedure described in McNamara and Buland (2004). The PSDs are binned in 1/8-octave interval periods and 1-dB interval power. Then, probability density functions (PDF) are constructed by normalizing each period-power bin by the total number of contributing segments (McNamara *et al.*, 2009).

As an example, Figure 2 shows the median power spectra for all the land and OBS stations of the network. The noise levels are compared to the global new high noise model (NHNM) and new low noise model (NLNM) of Peterson (1993), which are based on land observations. For frequencies lower than 0.1 Hz, the vertical-component noise levels are within the range of the NLNM and NHNM for the broadband stations in the Canary Islands and Morocco. The secondary microseismic peak (Longuet-Higgins, 1950; Hasselmann, 1963) is obscured on the noisier horizontal components and cannot be observed on the short-period OBS instruments. In the frequency band between 0.1 and 0.5 Hz, which contains the primary microseism, the land stations present, in general, lower noise levels than the OBS stations. In the short-period band (> 0.5 Hz), which is of interest to local seismicity studies, the noise levels are below the NHNM for most of the stations. However, there are some coastal stations in Morocco that exceed the NHNM level at 0.5-2 Hz, which is caused by wind-wave-induced near-shore secondary microseismic sources (Gimbert and Tsai, 2015). A pronounced noise peak is observed on all the OBS's vertical and horizontal components between 5 and 7 Hz. The OBS noise in the short-period band is usually related to the local weather conditions, marine mammals and anthropogenic sources, such as shipping noise or drilling activities. In this case, the recorded spectral peak is associated with the presence of an ocean-current-driven harmonic tremor that we will analyze below.

HIGH FREQUENCY SIGNALS IN OBS DATA

Ship propellers, whales, and drilling

Several signals were recorded that interfere with local earthquake detections by the OBS network. Nearby passing ships are easily identified on high-frequency spectrograms as multiple harmonics lasting for several hours over a diffuse broadband component (e.g., McKenna *et al.*, 2012; Wilcock *et al.*, 2014). Persistent spectral peaks from distant ships are also distinctly recognized. The Canary Channel is a region of high maritime traffic and we visually identified, on average, more than 3 signatures of individual ships per day during the 106-day OBS recording period (Figure 3a). Moreover, this region has a population of resident whales that can be found year-round. Therefore, numerous short-duration (1-s), regularly spaced fin whale vocalizations (e.g., Širović *et al.*, 2017) are nearly always visible in the OBS data and contribute to the ambient noise levels around 20 Hz (Figure 3b). Blue whale calls with duration of about 18 s and a dominant frequency of 16.8 Hz (e.g., Stafford *et al.*, 2005) can be also recognized on some OBS records (Figure 3d). Finally, signals related to the drilling activities were distinctly detected and recorded by all the instruments of the OBS network (Figure 3c). They correspond to airgun shots from a vertical seismic profile (VSP) operation in the exploration well.

Harmonic tremor

High-frequency OBS records are dominated by long-duration, harmonic waveforms. The tremors are visually recognized in all the three-component seismograms as well as in their spectrograms (Figure 4). Their amplitudes present a wide range of values, and they are higher on the horizontal components than on the vertical one. Sometimes, but not always, the signals can also be observed on the corresponding hydrophone spectrograms; however, they are not identified on the land seismometer recordings. The duration of tremors is variable and they usually occur in swarms that may last from few minutes up to several hours. The signals are highly monochromatic and peak between 5.5 Hz and 7.0 Hz. A weak higher frequency harmonic may be identified in some of the records. Spectral gliding (small short-term fluctuations in the fundamental and harmonic frequencies through time) is also observed in the spectrograms. The polarization is characterized by a stable behavior with one or two azimuths at each site during the entire deployment period.

Occurrence of harmonic tremors similar to those observed in this work has been reported in other volcanic and non-volcanic regions of the world, e.g., Pontoise and Hello (2002) offshore Ecuador, Tolstoy *et al.* (2002) near Axial volcano on the Juan de Fuca Ridge, Díaz *et al.* (2007) at the Galicia Margin, Monigle *et al.* (2009) at the 9º50' East Pacific Rise, Bazin *et al.* (2010) in Guadeloupe, French West Indies, and Franek *et al.* (2014) in the SW Barents Sea margin. Several hypotheses have been proposed, as discussed later, to explain their origin.

Short-duration events

We also observed few dozens or less (depending on the station) of short-duration (from about 0.5 s to 4 s), impulsive signals per day for each single OBS during the entire deployment period. Their spectra may peak at one or several discrete frequencies over a range up to the Nyquist frequency and peak amplitudes may vary several orders of magnitude. There is no evidence that these signals are recorded by more than one station, which suggests a very local source, as distances as short as 5 km separate the OBS sites. Recording of the signals on the pressure channel is variable, but the most energetic events are always recorded by the corresponding hydrophone. Although some of the recorded signals occur in clusters, most of them are single events. The microevents do not show secondary arrivals, and they present a regular amplitude decrease in the coda. Figure 5 shows some typical examples of the observed data, grouped into few types of events by visual inspection. Type A event, which is the most common, has broader frequency content. Type B has the longer durations and presents a resonant low frequency peak. Type C has a high frequency dominant peak that may vary among events. Particle motion analysis shows that there are not preferential directions. For some stations we observed strong horizontal motions that may be caused by horizontal transients and/or poor coupling on the sea floor.

The signal characteristics described above have already been reported in the literature, e.g., Buskirk *et al.* (1981) at several offshore experimental sites, including Alaska, the New Hebrides, the Marianas, northern California and Mexico; Díaz *et al.* (2007) at the Galicia Margin (North Atlantic Ocean); Tary *et al.* (2012) and Tsang-Hin-Sun *et al.* (2019) in the Sea of Marmara; Bowman and Wilcock (2014) at Deception Island volcano (Antarctica); Sgroi *et al.* (2014) in the western Ionian Sea; and Franek *et al.* (2017) in the western Svalbard shelf. Nevertheless, their origin still remains unclear.

NATURE OF THE HARMONIC TREMORS AND SHORT DURATION EVENTS

Figure 6 shows an example of the root mean square (RMS) tremor amplitudes recorded at all the OBS instruments using 10-second-long windows with no overlap for 3 hours of data filtered in the 5.5 to 7.0 Hz frequency band. The stations are sorted by deployment depth that ranges from 1,355 m for OB17 to 709 m for OB03. A lack of temporal coherence between stations is observed, which suggests a local origin of the sources. Unlike Pontoise and Hello (2002), tremor amplitude levels do not show a dependence on the depth of the OBS in our case.

Data inspection evidenced that tremors do not occur continuously, but they present a time periodicity. Figure 7a shows a comparative plot of the RMS amplitudes of the recorded signal and the measured sea level variation during 4 days of intense tremor activity at one site. Cross-spectral analysis yields a coherence value of 0.98 at semidiurnal frequency in this example. Autospectral analysis of the entire OBS data set shows that, besides the 12-hour periodicity, there are diurnal and fortnightly oscillations present as well (Figure 7b). The observed periodicities correspond to major tidal constituents, which supports a tidal modulation of tremor amplitudes.

To analyse the role of tidal current speed on the source mechanism of tremors, we computed the kinetic energy from the current-meter velocity recordings at the Eastern Boundary Current 4 (EBC4) mooring (e.g., Vélez-Belchí *et al.*, 2017). These instruments acquire velocity, temperature, salinity, and pressure data at a sampling time of 2 hours and are located close to the OBS network (Figure 1). Spectral analysis reveals coherent peaks between the kinetic energy records and the RMS tremor amplitudes at about 1, 2, 3, and 4 cycles/day (Figure 7c). This suggests a strong relationship between the occurrence of tremors and ocean currents.

To make a guess at the source of the short-duration signals we identified automatically the microshocks by means of FilterPicker, a short-term average (STA)/long-term average (LTA) phase detection algorithm (Lomax *et al.*, 2012). In our study, the recording of a large number of ship and marine mammals' signals, as well as the ubiquitous presence of the harmonic tremor, make it difficult to perform a systematic analysis of the time distribution of the short-duration events, which were obscured frequently both in time and in frequency domains. Therefore, we processed the data in the frequency band ranging from 9 Hz to 16 Hz, which proved to be the most adequate after careful testing on several randomly selected days. We got optimal trigger results, consistent with those from visual inspection, using the parameters 0.2 s for the filter window (T_{filter}), 4.0 s for the long-term window (T_{long}), 5.5 for the thresholds (S_1 and S_2), and 1 s for the time width (T_{up}).

Figure 8 (a) shows the detected average daily rate of microshocks for the entire deployment period as a function of the OBS depth. With a mean number of 91 events per day, station OB09 (1,126-meter water depth) is the noisiest, whereas OB01 (900-meter water depth) presents the lowest average rate with 11 microevents per day. The average number of short-duration events does not show a clear dependence on the OBS depth. Figure 8 (b) plots examples of the temporal distribution of the number of microshocks per day at three sites. The event rate distribution is variable from site to site and it presents a 12.4-hour cycle at 9 out of the total 17 OBS, which may indicate a relationship with the semidiurnal (M2) tidal constituent. The rest of the stations do not present any clear periodicity. A depth dependence of the two groups of stations, which would suggest a relationship with daylight (e.g., Buskirk *et al.*, 1981), is not observed. The hourly distribution of the short-duration signals (Figure 8c) is also variable among stations and it presents some clustering at random times.

RECORDED SEISMICITY

Continuous data from the land network, including data from permanent and temporary stations, were initially processed in real time using both SeisComP3 and Earthworm earthquake processing softwares (see Data and Resources). After recovery of the OBS network in February 2015, the marine data were added to the database and we played back the whole data set using Earthworm. The numerous interfering signals recorded by the OBS network generated a large number of false detections that we removed visually. Seismic phases were then manually re-picked using Seisan analysis software (see Data and Resources). We also used Seisan to locate the events by means of Hypocenter location algorithm (Lienert and Havskov, 1995) and for the determination of local magnitude. We used a regional 1D layered velocity model utilized by the IGN for routine earthquake location in the Canary Islands, with a v_P/v_S of 1.75.

A total of 24 earthquakes with local magnitudes ranging from 0.9 to 2.5 were detected during the 12-month period of seismic monitoring. Among these, only two events were located to the east of the Canary Ridge (Figure 9a). The first event, with local magnitude M=1.7, occurred on January 3, 2015 (during the period of drilling activities) but it was located at a distance of 70 km from the drilling site. The second one, with local magnitude M=1.8, occurred on March 30, 2015 (11 weeks after the end of the drilling operations) at 19 km distance from the drilling well (Figure 9b). Figure 3(e) shows an example of one OBS seismogram and spectrogram.

DISCUSSION AND CONCLUSIONS

Seismicity rates

The low seismicity levels recorded by the temporary network are in accordance with the seismicity records available in the region. The Canary Islands present low-to-moderate magnitude seismic activity of tectonic and volcanic origin, most of which is spatially distributed to the west of the Canary Ridge. Seismicity decreases to the east of the archipelago, from the Canary Ridge toward the African continent. For the entire 12-month seismic monitoring period of the network, we did not detect any increase of the seismicity rate that could be associated with the hydrocarbon exploration activities performed in the Canary Channel (Figure 9a). The long term surrounding seismicity also remained stable in this area after the drilling operations (Figure 9b). The deployment of the temporary network supplemented the earthquake catalogue in the eastern Canary Islands by the addition of 12 earthquakes, which represents an increase of 80% with respect to the events reported by the Spanish permanent network (IGN) catalogue in the same region (Figure 9c).

Harmonic tremor

The harmonic tremors reported in other regions (e.g., Pontoise and Hello, 2002; Tolstoy *et al.*, 2002; Díaz *et al.*, 2007; Monigle *et al.*, 2009; Bazin *et al.*, 2010; Franek *et al.*, 2014) have been associated with gas venting and/or resonance of fluid-filled cracks. The geological setting of the Canary Channel would support an interpretation of the harmonic tremors in terms of resonant vibrations associated with gas seepage. However, the same instruments recorded similar signals during other campaigns in different regions of the world (Marine Technology Unit-CSIC, pers. comm.). Olofsson (2010) investigated several types of noise recordings usually observed in seismic marine data sets. Arguing in a different way, he attributed his noise type 6, which is very similar to the harmonic tremor observed in this work, to flagpole resonant vibrations induced by water currents. In this study, the spatial distribution of the recorded RMS amplitudes at all the OBS sites does not follow any clear pattern. The location of the mounds and pockmarks imaged in the Canary Channel does not correlate with the distribution of the noisiest stations either (Figure 10a). The band pass-filtered RMS time series present tidal signatures of the semi-diurnal, diurnal and spring-neap cycles (Figure 7b). This result is consistent with harmonic tremors being driven by water currents, which are modulated by tides. For the period from two hours to one day, the spectral analysis of the RMS time series and the kinetic energy computed from current-meter velocity recordings show coherent peaks at diurnal and semidiurnal cycles (Figure 7c). The 6 h 12 min modulation of tremors (4 cycles/day), which corresponds to the time period over which current speed reverses direction, is dominant at several OBS sites. These observations indicate that the tremor activity results from bottom water currents in the Canary Channel, which may induce resonances on the instrument-seafloor system.

Short-duration events

The lack of correlation between records of adjacent stations may discard a tectonic origin of the short-duration signals detected by the OBS network. A supporting evidence may be that, in addition to the hydrophones, all the geophones of the marine network recorded the airgun shots from the VSP travelling through the water and through the ground; however, their amplitudes are one order of magnitude lower than the strongest short-duration events recorded on the OBS channels (Figures 3c and 5), which were local to each station. Moreover, the lack of secondary arrivals would imply that *P* and *S* waves arrivals overlap, so the very small earthquakes would occur very close (at distances of the order of meters) from every station. But widespread active faulting is not in agreement with the observed seismicity pattern of the eastern Canary Islands, where very few tectonic features have been described (González de Vallejo *et al.*, 2006). The short-duration signals recorded on the OBS stations share common signatures among the different sites of our deployment, and also with the microevents recorded by other instruments in different geotectonic settings of the world. They have been usually associated with biologic sources striking the instruments (Buskirk *et al.*, 1981; Brocher and Iwatake, 1982; Ostrovsky, 1989; Bowman and Wilcock, 2014). Other interpretations include fluid-filled crack sources (Díaz *et al.*, 2007), gas seepage (e.g., Tary *et al.*, 2012; Tsang-Hin-Sun *et al.*, 2019); hydraulic fracturing (e.g., Sgroi *et al.*, 2014); and combined processes of fracturing related to gas seepage and vibration (Franek *et al.*, 2017). In our study, we cannot exclude completely the possibility that gas related processes may be involved in the source mechanism of some short-duration events, as the OBS instruments are located within a salt diapiric field, where pockmarks formed by the expulsion of thermogenic fluids and mounds built-up by hydrocarbon and oil seeps along the crests of the salt diapirs have been imaged and photographed (see Figures 5 and 7 of Acosta *et al.*, 2005). However, the spatial distribution of the average number of microshocks per day does not show any clear pattern (Figure 10b). Moreover, it is difficult to explain the very large amplitudes of many short-duration events in terms of natural shallow sources located close to every instrument. Oloffson (2010) classified similar signals to those observed here as type 5 noises and discussed their potential source mechanisms. He concluded that sea life, particles carried by the water currents, or loose parts at the instrument units were likely the cause of the noise signals. Based on our observations, we also believe that the transients are probably caused by environmental factors in the Canary Channel. The recorded short-duration events are similar to the signals obtained in the transient pull tests reported by Trehu (1985). And induced nonacoustic mechanical vibrations may produce noise outputs on hydrophone recordings, too (Audoly and Giangreco, 1992). Marine life and transporting ocean currents may cause sudden impulsive forces acting on the instruments. Turbulences triggered by bottom water currents that exceed 22 cm/s at 1,319 m depth in this area could be the source of microshock clustering (Chang *et al.*, 2016). Further study is required to better understand these possible processes.

DATA AND RESOURCES

The continuous waveform dataset of the temporary seismic network is available upon request (contact person: A. Ugalde, a.ugalde@icm.csic.es). Seismic data were processed using both SeisComP3 (https://www.seiscomp3.org/; last accessed June 2018) and Earthworm earthquake processing softwares (http://www.earthwormcentral.org/; last accessed June 2018). Seismic phases were analyzed using Seisan software (Havskov and Ottemöller, 1999; http://www.seisan.info/, last accessed June 2018). The IGN catalogue is publicly available and was searched through http://www.ign.es/web/ign/portal/sis-catalogo-terremotos (last accessed June, 2018). Pedro Vélez-Belchí of the Spanish Institute of Oceanography (http://www.ieo.es; last accessed June, 2018) provided us with the current-meter recordings from EBC4 mooring. Tidal data were obtained from Puertos del Estado (http://www.puertos.es/es-es/oceanografia/; last accessed June 2018). Several figures were prepared using the Generic Mapping Tools (GMT) software (Wessel *et al.*, 2013) and the Java application Swarm (https://volcanoes.usgs.gov/software/swarm/; last accessed June 2018). Bathymetric data was provided by EMODnet (2018).

ACKNOWLEDGMENTS

We appreciate the help of Jaime Arranz and Orlando Hernández from the Geo-park "La Casa de los Volcanes" during the field campaign in Lanzarote and Fuerteventura. We are also grateful to the Spanish General State Administration Insular Directorate for the logistic help. We thank the Marine Technology Unit (UTM-CSIC) and the RV García del Cid for the deployment and recovery of the OBS instruments. Thanks are also due to Prof. Mimoun Harnafi and the personnel of the Institut Scientifique of Mohammed V University (Agdal-Rabat) for installing the land seismic network in southern Morocco. The Editor and two anonymous reviewers provided constructive comments and suggestions that greatly improved the manuscript. This research was funded by Repsol Project GEOMARGEN-3.

REFERENCES

Acosta J., E. Uchupi, A. Muñoz, P. Herranz, C. Palomo, M. Ballesteros, and ZEE Working Group (2005). Salt Diapirs, Salt Brine Seeps, Pockmarks and Surficial Sediment Creep and Slides in the Canary Channel off NW Africa, in: Clift P., Acosta J. (eds) *Geophysics of the Canary Islands*, Springer, Dordrecht, doi: 10.1007/1-4020-4352-X_2.

Audoly, E. and C. Giangreco (1992). A study of the output of a hydrophone fixed on avibrating structure. *Journal de Physique IV Colloque* **02 (C1)** C1-973-C1-976.<10.1051/jp4:19921213>. <jpa-00251180>.

Banda, E., Dañobeitia, J.J., Suriñach, E., and J. Ansorge (1981). Features of crustal structure under the Canary Islands, *Earth Planet. Sci. Lett.* **55** 11–24, doi: 10.1016/0012-821X(81)90082-0.

Bazin, S., N. Feuillet, C. Duclos, W.Crawford, A. Nercessian, M. Bengoubou-Valérius, F. Beauducel, and S.C. Singh (2010). The 2004–2005 Les Saintes (French West Indies) seismic aftershock sequence observed with ocean bottom seismometers, *Tectonophysics* **489** 91-103, doi:10.1016/j.tecto.2010.04.005.

BOE (2014). *Boletín Oficial del Estado*, Núm. 196, Sec. III Pág 64826, Miércoles 13 de agosto de 2014 (in Spanish).

Bowman, D. C. and W. S. D. Wilcock (2014). Unusual signals recorded by ocean bottom seismometers in the flooded caldera of Deception Island volcano: volcanic gases or biological activity? *Antarctic Science* **26**(3) 267–275, doi:10.1017/S0954102013000758.

Brocher, T. M. and B. T. Iwatake (1982). Sources of low-frequency ambient seafloor noise on a continental shelf, *Bull. Seism. Soc. Am.* **72**(4) 119-1142.

Buskirk, R. E., C. Frohlich, G. V. Latham, A. T. Chen, and J. Lawton (1981). Evidence that biological activity affects ocean bottom seismograph recordings, *Mar. Geophys. Res.* **5** 189–205, doi: 10.1007/BF00163479.

Carracedo, J. C. (1999). Growth, structure, instability and collapse of Canarian volcanoes and comparisons with Hawaiian volcanoes, *J. Vol. Geoth. Res.* **94** 1–19, doi: 10.1016/S0377-0273(99)00095-5.

Chang, E. T. Y., B. F. Chao, G.-Y. Chen, and J.-M. Liau (2016). Internal tides recorded at ocean bottom off the coast of Southeast Taiwan. *J. Geophys. Res. Oceans* **121** 3381–3394, doi:10.1002/2015JC011370.

Díaz, J., J. Gallart, and O. Gaspà (2007). Atypical seismic signals at the Galicia Margin, North Atlantic Ocean, related to the resonance of subsurface fluid-filled cracks, *Tectonophysics* **433** 1–13, doi:10.1016/j.tecto.2007.01.004.

Eaton, D. (2018). *Passive Seismic Monitoring of Induced Seismicity: Fundamental Principles and Application to Energy Technologies*, Cambridge University Press, doi: 10.1017/9781316535547.

EMODnet Bathymetry Consortium (2018). *EMODnet Digital Bathymetry (DTM)*, http://doi.org/10.12770/18ff0d48-b203-4a65-94a9-5fd8b0ec35f6.

Foulger, G. R., M. P. Wilson, J. G. Gluyas, B. R. Julian, and R. J. Davies (2018). Global review of human-induced earthquakes, *Earth-Science Reviews* **178** 438-514, doi: 10.1016/j.earscirev.2017.07.008.

Franek, P., A. Plaza-Faverola, J. Mienert, S. Buenz, B. Ferré, and A. Hubbard (2017). Microseismicity linked to gas migration and leakage on the Western Svalbard Shelf. *Geochem. Geophys. Geosys.* **18** 4623–4645, doi:10.1002/2017GC007107.

Franek, P., J. Mienert, S. Buenz, and L. Géli (2014), Character of seismic motion at a location of a gas hydrate bearing mud volcano on the SW Barents Sea margin, *J. Geophys. Res. Solid Earth* **119** 6159–6177, doi:10.1002/2014JB010990.

Gimbert, F. and V. C. Tsai (2015). Predicting short-period, wind-wave-generated seismic noise in coastal regions, *Earth Planet. Sci. Lett.* **426** 280-292, doi:10.1016/j.epsl.2015.06.017.

González de Vallejo, L. I., J. García-Mayordomo, and J. M. Insua (2006). Probabilistic seismic-hazard assessment of the Canary Islands, *Bull. Seism. Soc. Am.* **96**(6) 2040–2049, doi:10.1785/0120050139.

Hasselmann, K. (1963). A statistical analysis of the generation of microseisms, *Rev. Geophys.* **1**(2) 177–210, doi:10.1029/RG001i002p00177.

Havskov, J., and L. Ottemöller (1999). SeisAn earthquake analysis software, *Seism. Res. Lett.* **70** 532−534, doi:10.1785/gssrl.70.5.532.

Lienert, B. R. E., and J. Havskov (1995). A computer program for locating earthquakes both locally and globally, *Seismol. Res. Lett.* **66** 26-36, doi: 10.1785/gssrl.66.5.26.

Lomax, A., C. Satriano and M. Vassallo (2012). Automatic picker developments and optimization: FilterPicker - a robust, broadband picker for real-time seismic monitoring and earthquake early-warning, *Seism. Res. Lett.* , **83**, 531-540, doi: 10.1785/gssrl.83.3.531.

Longuet-Higgins, M. S. (1950). A theory of the origin of microseisms, *Philos. Trans. R. Soc. A* **243** 1–35, doi: 10.1098/rsta.1950.0012.

McKenna, M. F., D. Ross, S. M. Wiggins, and J. A. Hildebrand (2012). Underwater radiated noise from modern commercial ships, *J. Acoust. Soc. Am.* **131**(1) 92-103, doi: 10.1121/1.3664100.

McNamara, D. E., and R. P. Buland (2004). Ambient noise levels in the continental United States, *Bull. Seismol. Soc. Am.* **94** 1517–1527, doi: 10.1785/012003001.

McNamara, D. E., C. R. Hutt, L. S. Gee, H. M. Benz, and R. P. Buland (2009). A method to establish seismic noise baselines for automated station assessment, *Seismol. Res. Lett.* **80** 628–637, doi:10.1785/gssrl.80.4.628.

McNamara, D. E., and R. I. Boaz (2011). *PQLX: A seismic data quality control system description, applications, and users manual*, U.S. Geological Survey Open-File Rept. 2010-1292, 41 pp.

Monigle, P. W., D. R. Bohnenstiehl, M. Tolstoy, and F. Waldhauser (2009). Seismic tremor at the 9_500N East Pacific Rise eruption site, *Geochem. Geophys. Geosyst.* **10**, doi:10.1029/2009GC002561.

National Research Council (2013). *Induced Seismicity Potential in Energy Technologies*. The National Academies Press, Washington DC, doi:10.17226/13355.

Oloffson, B. (2010). Marine ambient seismic noise in the frequency range 1-10 Hz, *The Leading Edge* **29**(4) 418-435, doi:10.1190/1.3378306.

Ostrovsky, A. A. (1989). The estimation of Ocean Bottom Seismographs' coupling characteristics by means of microshock recordings, *Marine Geophysical Researches* **11** 119-127, doi:10.1007/BF00285663.

Peterson, J. (1993). *Observation and modeling of seismic background noise*, U.S. Geological Survey Open-File Rept. 1993-322, 95 pp.

Pontoise, B. and Y. Hello (2002). Monochromatic infra-sound waves recorded offshore Ecuador: possible evidence of methane release, *Terra Nova* **14** 425–435, doi: 10.1046/j.1365-3121.2002.00437.x.

Rivera, J., M. Canals, G. Lastras, N. Hermida, D. Amblas, B. Arrese, P. Martín-Sosa, and J. Acosta (2016). Morphometry of Concepcion Bank: Evidence of Geological and Biological Processes on a Large Volcanic Seamount of the Canary Islands Seamount Province. *PLoS ONE* **11**(5), doi:10.1371/journal.pone.0156337.

Sgroi, T., S. Monna, D. Embriaco, G. Giovanetti, G. Marinaro, and P. Favali (2014). Geohazards in the Western Ionian Sea: Insights from non-earthquake signals recorded by the NEMO-SN1 seafloor observatory. *Oceanography* **27**(2) 154–166, doi:10.5670/oceanog.2014.51.

Širović, A., E. M. Oleson, J. Buccowich, A. Rice, and A. R. Bayless (2017). Fin whale song variability in southern California and the Gulf of California, *Scientific Reports* **7**(1), doi: 10.1038/s41598-017-09979-4.

Stafford, K. M., S. E. Moore, and C. G. Fox (2005). Diel variation in blue whale calls recorded in the eastern tropical Pacific, *Animal Behaviour* **69** 951–958, doi:10.1016/j.anbehav.2004.06.025.

Tary, J.B., L. Géli, C. Guennou, P. Henry, N. Sultan, N. Çağatay, and V. Vidal (2012). Microevents produced by gas migration and expulsión at the seabed: a study based on sea bottom recordings from the Sea of Marmara. *Geophys. J. Int.* **190** 993–1007, doi: 10.1111/j.1365-246X.2012.05533.x.

Tolstoy, M., F. L. Vernon, J. A. Orcutt, and F. K. Wyatt (2002). Breathing of the seafloor: Tidal correlations of seismicity at Axial volcano, *Geology* **30** 503–506, doi: 10.1130/0091-7613(2002)030<0503:BOTSTC>2.0.CO;2.

Trehu, A. M. (1985). Coupling of ocean bottom seismometers to sediment: results of tests with the U.S. Geological Survey ocean bottom seismometer, *Bull. Seism. Soc. Am.* **75** 271-289.

Tsang-Hin-Sun, E., E. Batsi, F. Klingelhoefer, L. Géli (2019). Spatial and temporal dynamics of gas-related processes in the Sea of Marmara monitored with ocean bottom seismometers, *Geophys. J. Int.* **216** 1989–2003, https://doi.org/10.1093/gji/ggy535.

Vélez-Belchí, P., M. D. Pérez-Hernández, M. Casanova-Masjoan, L. Cana, and A. Hernández-Guerra (2017). On the seasonal variability of the Canary Current and the Atlantic Meridional Overturning Circulation, *J. Geophys. Res. Oceans* **122**, 4518–4538, doi:10.1002/2017JC012774.

Wilson, M. P., G. R. Foulger, J. G. Gluyas, R. J. Davies, and B. R. Julian (2017). *HiQuake*: The Human-Induced Earthquake Database, *Seism. Res. Lett.* **88** (6), 1560–1565, doi: https://doi.org/10.1785/0220170112.

Wessel, P., W. H. F. Smith, R. Scharroo, J. F. Luis, and F. Wobbe (2013). Generic Mapping Tools: Improved version released. *EOS Trans. AGU* **94** 409-410, doi: 10.1002/2013EO450001.

W. S. D. Wilcock, K. M. Stafford, R. K. Andrew, and R. I. Odom (2014). Sounds in the ocean at 1-100 Hz, *Annu. Rev. Mar. Sci.* **6** 117–40, doi:10.1146/annurev-marine-121211-172423.

LIST OF FIGURE CAPTIONS

Figure 1. Seismicity map of the eastern Canary Islands region from 1976 to 2014 according to the IGN catalogue (see Data and Resources). The temporary land and OBS stations are plotted, together with the permanent seismic stations of the Spanish National Seismic Network. Three land stations in Morocco are located outside the plotted area. The inverted solid triangles are the accelerometric stations. Earthquakes are scaled by magnitude in the range $1.0 \leq m_bLg \leq 4.6$.

Figure 2. Median of the power spectral density (PSD) in dB referred to $(m/s^2)^2/Hz$ for the temporary stations located in the Canary Islands (top), the OBS network (middle) and the land stations in Morocco (bottom). The vertical component (left) and the geometric mean of the horizontal components (right) are plotted together with the New Low Noise Model (NLNM) and New High Noise Model (NHNM) of Peterson (1993).

Figure 3. Examples of high-pass-filtered OBS waveforms and spectrograms in units of log[nm^2/Hz] for channel EHZ (vertical component) and log[Pa^2/Hz] for channel EHH (hydrophone) for (a) ship noise; (b) fin whale call; (c) airgun shots; (d) blue whale call; and (e) a local earthquake on January 3, 2015. The spectrograms were calculated using 10-second-long (a), 2-second-long (b, c, d) and 1-second-long (d) 75% overlapping windows for the Fast Fourier Transform. Note the different time and amplitude scales.

Figure 4. Example of time series (2 Hz high-pass filtered) and spectrograms showing tremors recorded at station OB06. The spectrograms, in units of log[nm^2/Hz] for channel EHZ and log[Pa^2/Hz] for channel EHH, are calculated using 10-second-long, 75% overlapping windows for the Fast Fourier Transform. The fundamental and one harmonic frequencies show small fluctuations with time (gliding) around 6 Hz. In this example the tremors can be identified on the vertical (EHZ) and hydrophone (EHH)

channels. The particle motion (bottom) is consistent over the duration of the tremor and shows one azimuthal direction.

Figure 5. Examples of three different types of short-duration signals observed: (a) Type A, (b) type B, and (c) type C. The vertical-component raw seismogram (EHZ) and the high-pass-filtered hydrophone channel (EHH) are plotted. The bottom insets show the amplitude of the Fast Fourier Transform of the geophone channel (EHZ). The particle motion for the vertical and non-oriented horizontal components is also shown.

Figure 6. Root mean square (RMS) amplitudes computed using non-overlapping, 10-second-long windows for 3 hours of vertical-component recordings on January 3, 2015. The signals are band pass filtered between 5.5 Hz and 7.0 Hz. The stations are sorted by the depth of the deployment. It is noted the lack of temporal coherence between stations. In this example, OB02 presents high RMS amplitudes; however, the tremor is not recorded at OB03, which is also shallow and is located at a distance of 7.4 km from OB02.

Figure 7. (a) Example of the vertical-component, 5.5-7.0 Hz bandpass-filtered, root mean square (RMS) amplitudes computed using 1-hour-long consecutive windows for 4 days of recordings at station OB06 (solid line) and sea level data from the tide gauge located at Arrecife (Lanzarote) harbor (dashed line); (b) Power spectral density (PSD) of the 5.5-7.0 Hz bandpass-filtered, RMS amplitude time series for the entire operation period of station OB09. Semidiurnal (12.3 hours), diurnal (1 day and 26 hours) and fortnightly (14.2 days) dominant periods correspond to the tidal constituents M2, K1, O1 and the spring-neap cycle, respectively; and (c) comparison of the PSD of the kinetic energy time series from EBC4 mooring at 1,319 m depth (black) and the 5.5-7.0 Hz band pass-filtered, RMS amplitude time series from station OB15 at 1,251 m (grey). The dominant peak at this station occurs at 6 h 12 min.

Figure 8. (a) Average number of short-duration events (SDE) per day as a function of OBS depth. The OBS number is also plotted; (b) total number of SDE per day; and (c) total number of SDE per hour.

Figure 9. (a) Events recorded by the temporary network from 18/11/2014 to 07/10/2015 together with the earthquakes included in the IGN catalogue (see Data and Resources) for the years 1976 to 2014 and 2015 to 2018. Earthquakes are scaled by magnitude in the range $1.0 \leq m_bLg \leq 4.6$. The dashed circle encloses the threshold area of radius 75 km from the drilling site defined by the traffic-light warning protocol. Permanent and temporary stations are plotted as well as the drilling location (see the legend in Figure 1); (b) long term seismicity located inside the traffic-light warning protocol threshold area as a function of time and distance to the drilling site. The gray bar marks the drilling operation period; (c) difference between the number of earthquakes per day recorded by the temporary network and those included in the IGN catalogue in the whole study area for the monitoring period, starting on September 29, 2014. Negative values represent earthquakes included in the IGN catalogue that were not located by the temporary network. The plus symbols mark the earthquakes included in both catalogues.

Figure 10. (a) Averaged noise at the OBS network in the 5.5-7 Hz frequency band, for the entire 3-month recording period; and (b) average number of short-duration events (SDE) per day.

Figure 1

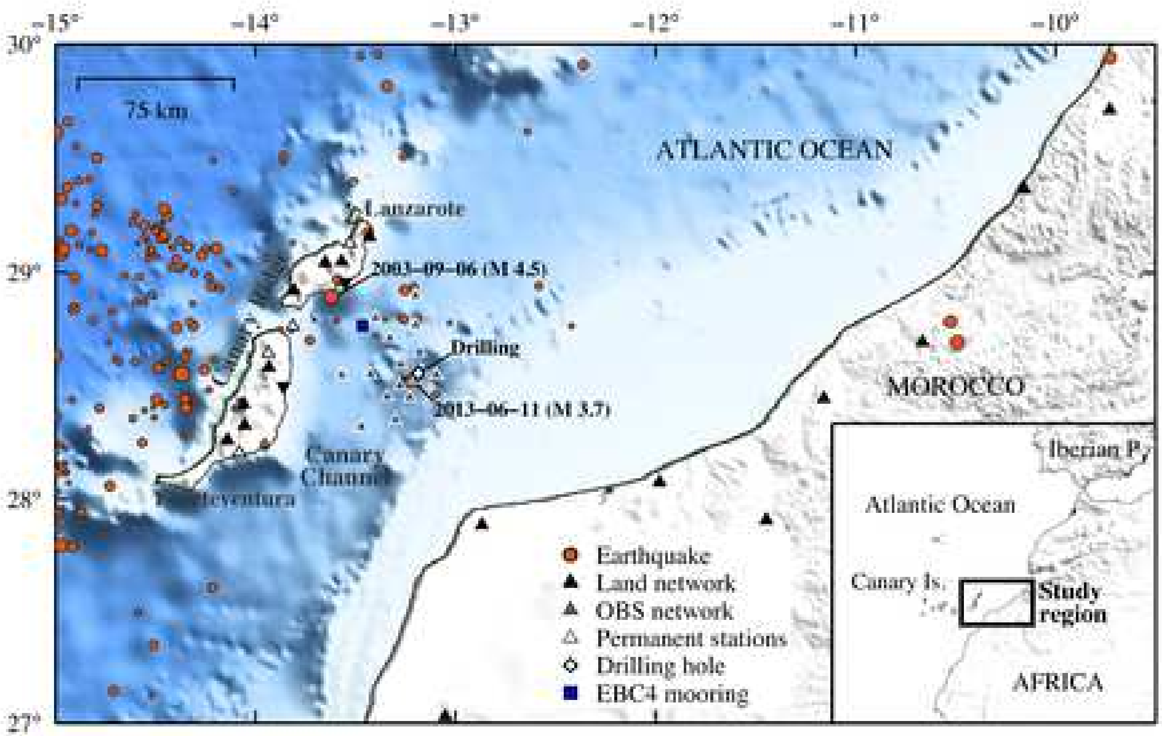
−15°
−14°
−13°
−12°
−11°
−10°
30°
29°
28°
27°
75 km
ATLANTIC OCEAN
Lanzarote
2003−09−06 (M 4.5)
Drilling
2013−06−11 (M 3.7)
Canary
Channel
MOROCCO
Earthquake
Land network
OBS network
Permanent stations
Drilling hole
EBC4 mooring
Iberian P.
Atlantic Ocean
Canary Is.
Study
region
AFRICA

Figure 2

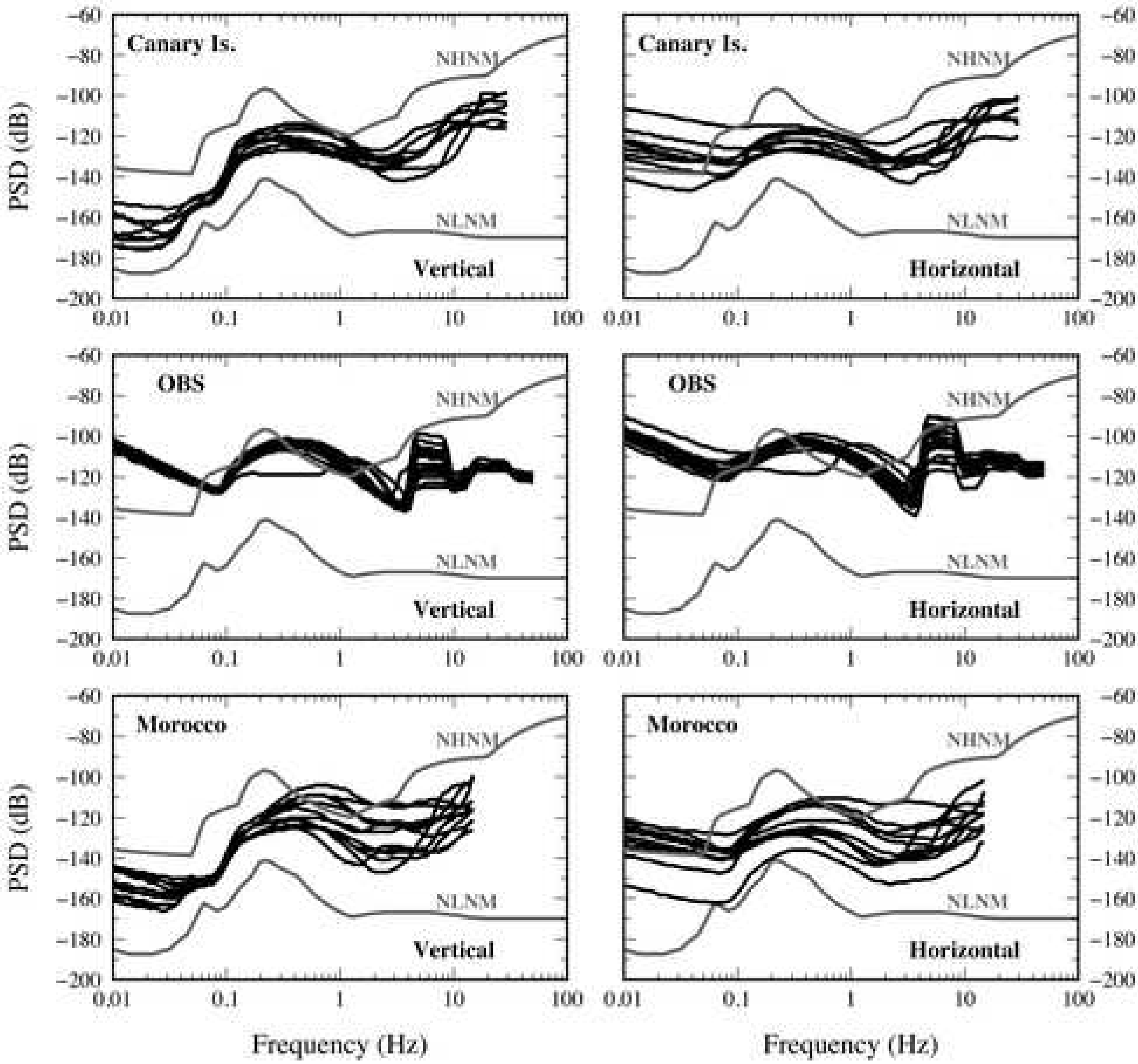

Canary Is.
NHNM
NLNM
Vertical
Horizontal
OBS
Morocco
PSD (dB)
Frequency (Hz)
-60
-80
-100
-120
-140
-160
-180
-200
0.01
0.1
1
10
100

Figure 3

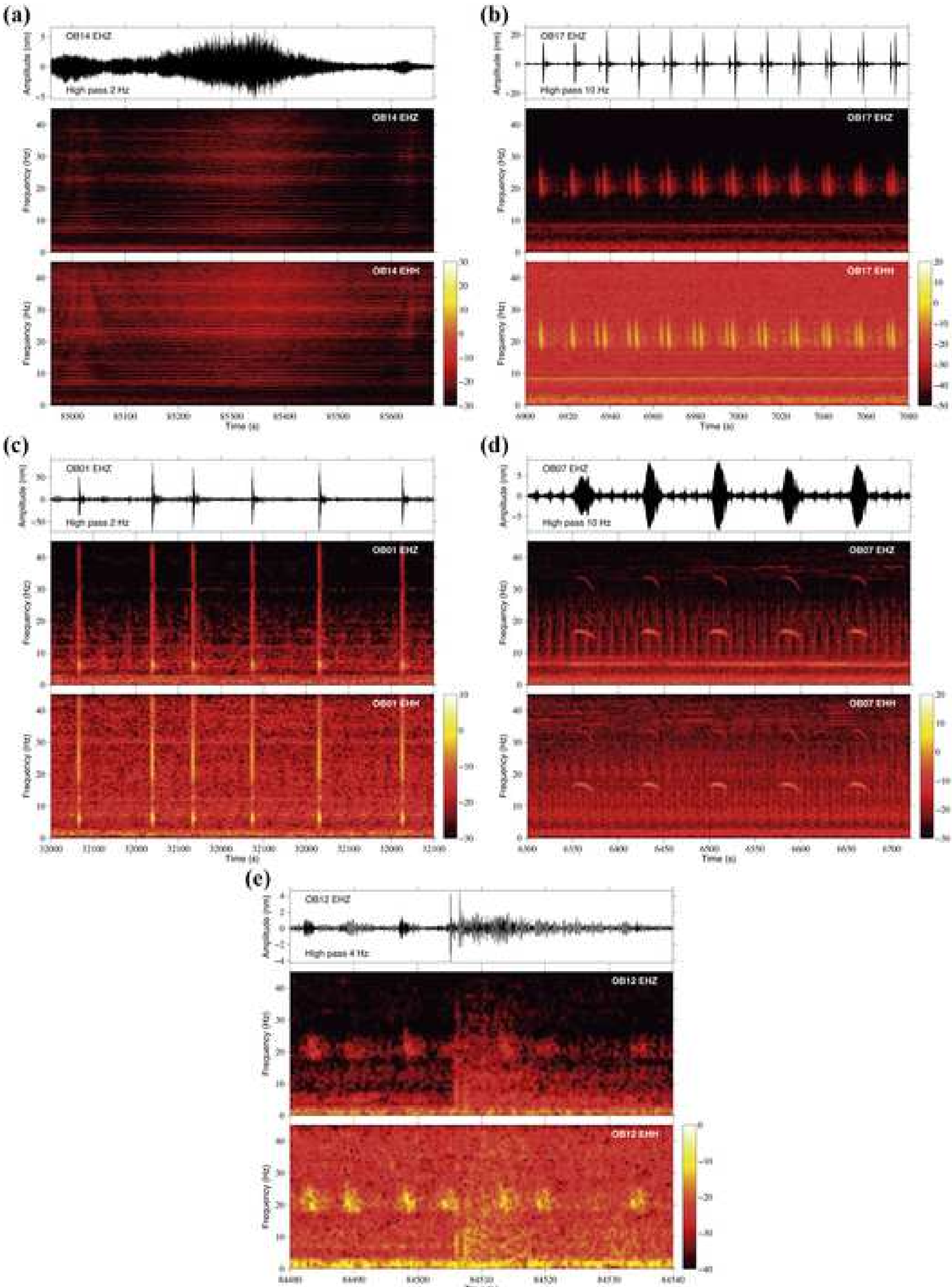
(a)
OB14 EHZ
High pass 2 Hz
OB14 EHZ
OB14 EHH
(b)
OB17 EHZ
High pass 10 Hz
OB17 EHZ
OB17 EHH
(c)
OB01 EHZ
High pass 2 Hz
OB01 EHZ
OB01 EHH
(d)
OB07 EHZ
High pass 10 Hz
OB07 EHZ
OB07 EHH
(e)
OB12 EHZ
High pass 4 Hz
OB12 EHZ
OB12 EHH
Amplitude (nm)
Frequency (Hz)
Time (s)

Figure 4

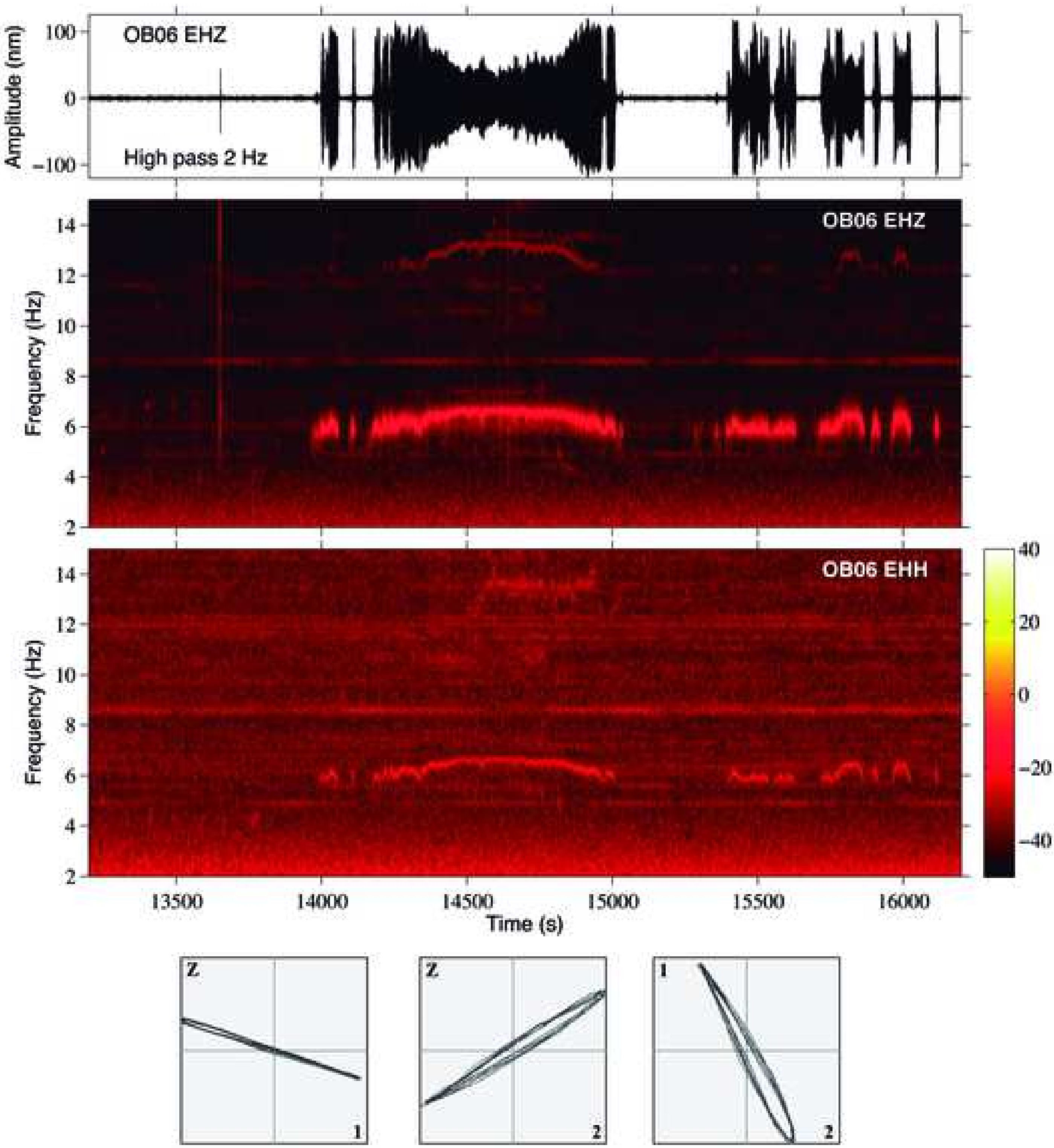

OB06 EHZ
High pass 2 Hz
Amplitude (nm)
100
0
-100
OB06 EHZ
Frequency (Hz)
14
12
10
8
6
4
2
OB06 EHH
Frequency (Hz)
40
20
0
-20
-40
13500
14000
14500
15000
15500
16000
Time (s)
Z
1
Z
2
1
2

Figure 5

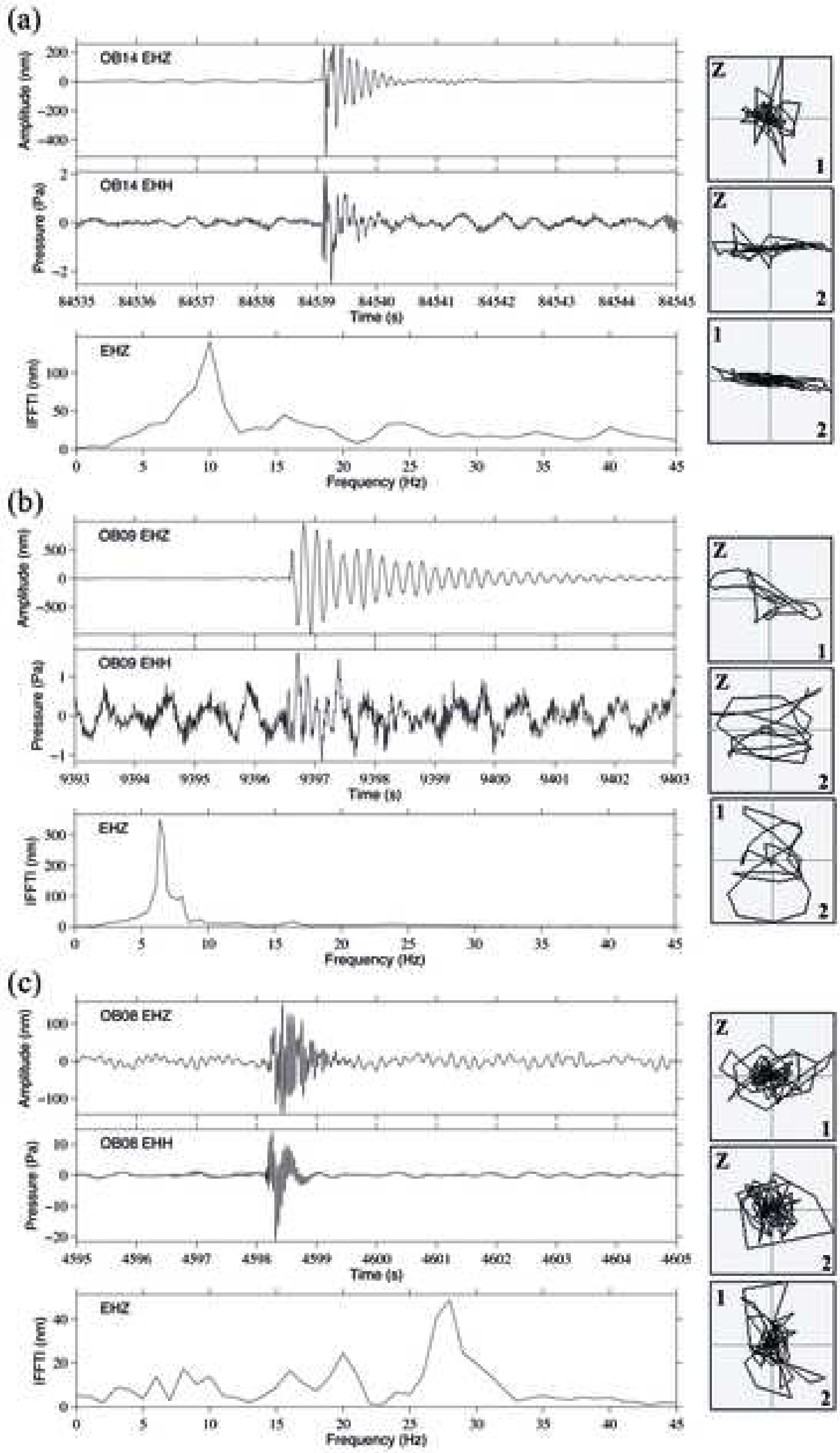
(a)
OB14 EHZ
Amplitude (nm)
OB14 EHH
Pressure (Pa)
Time (s)
EHZ
|FFT| (nm)
Frequency (Hz)
(b)
OB09 EHZ
Amplitude (nm)
OB09 EHH
Pressure (Pa)
Time (s)
EHZ
|FFT| (nm)
Frequency (Hz)
(c)
OB08 EHZ
Amplitude (nm)
OB08 EHH
Pressure (Pa)
Time (s)
EHZ
|FFT| (nm)
Frequency (Hz)

Figure 6

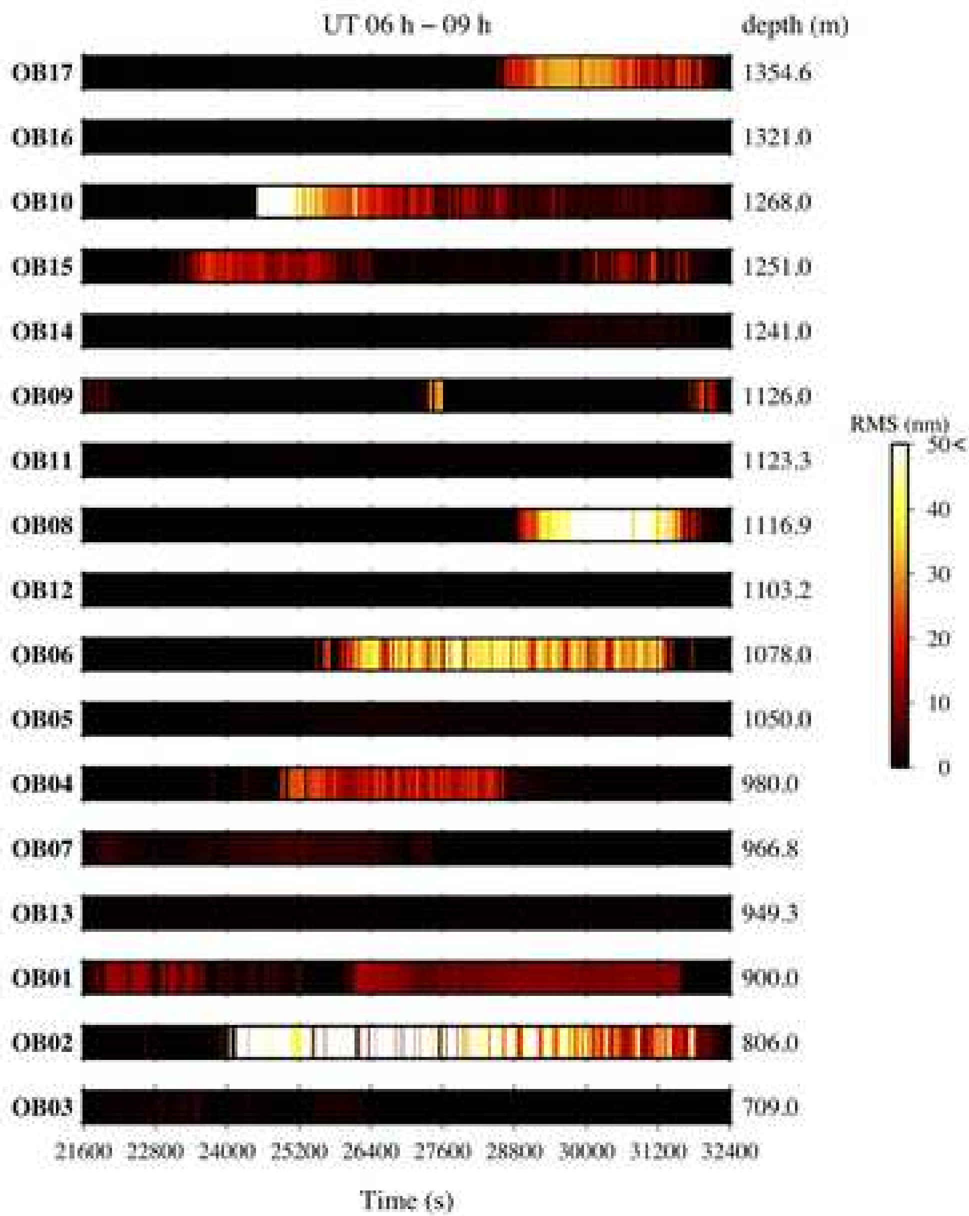
UT 06 h – 09 h
depth (m)
OB17
OB16
OB10
OB15
OB14
OB09
OB11
OB08
OB12
OB06
OB05
OB04
OB07
OB13
OB01
OB02
OB03
1354.6
1321.0
1268.0
1251.0
1241.0
1126.0
1123.3
1116.9
1103.2
1078.0
1050.0
980.0
966.8
949.3
900.0
806.0
709.0
21600
22800
24000
25200
26400
27600
28800
30000
31200
32400
Time (s)
RMS (nm)
50<
40
30
20
10
0

Figure 7

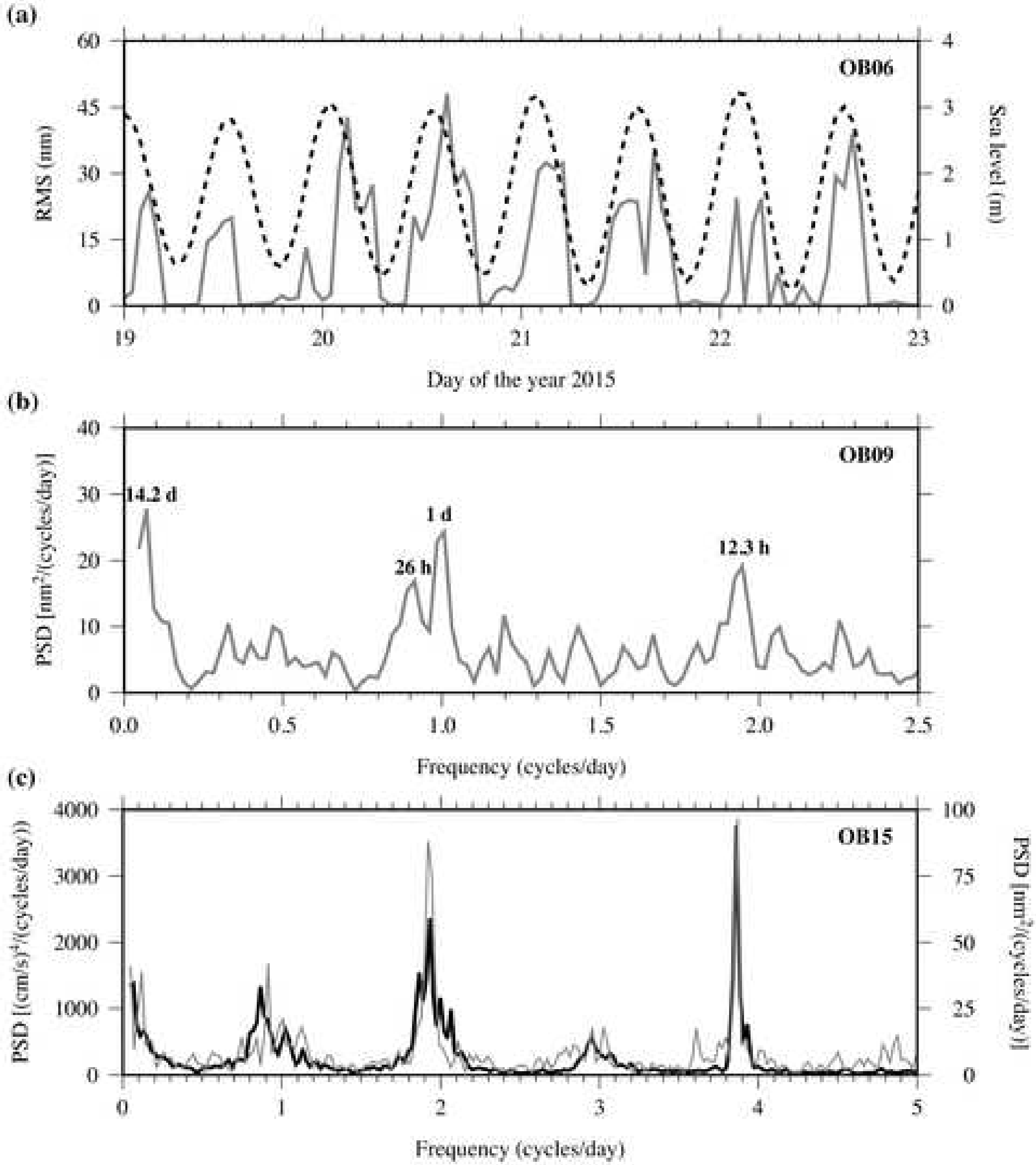

(a)
OB06
RMS (nm)
Sea level (m)
Day of the year 2015
(b)
OB09
PSD [nm²/(cycles/day)]
14.2 d
1 d
26 h
12.3 h
Frequency (cycles/day)
(c)
OB15
PSD [(cm/s)²/(cycles/day)]
PSD [nm²/(cycles/day)]
Frequency (cycles/day)

Figure 8

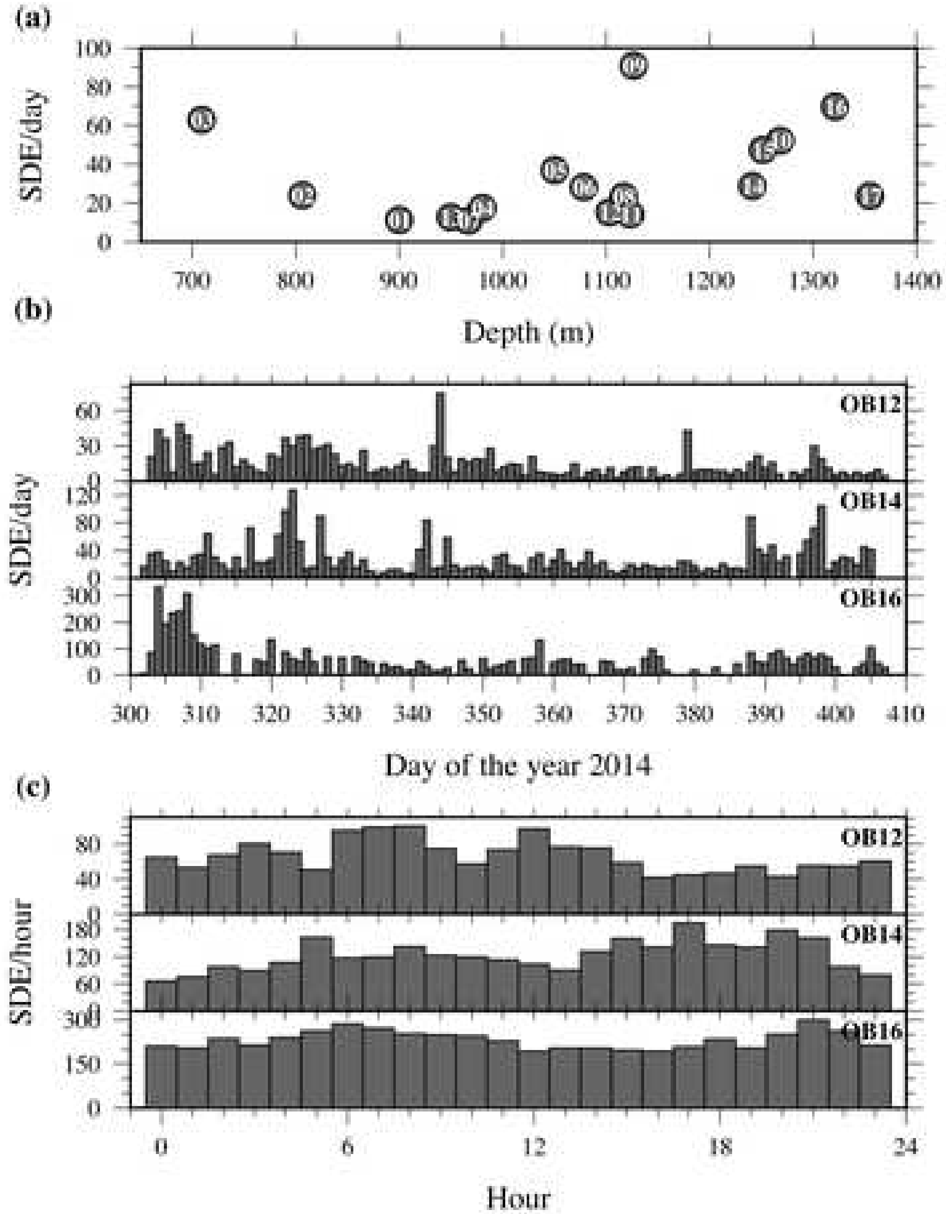

(a)
SDE/day
Depth (m)
(b)
SDE/day
OB12
OB14
OB16
Day of the year 2014
(c)
SDE/hour
OB12
OB14
OB16
Hour

Figure 9

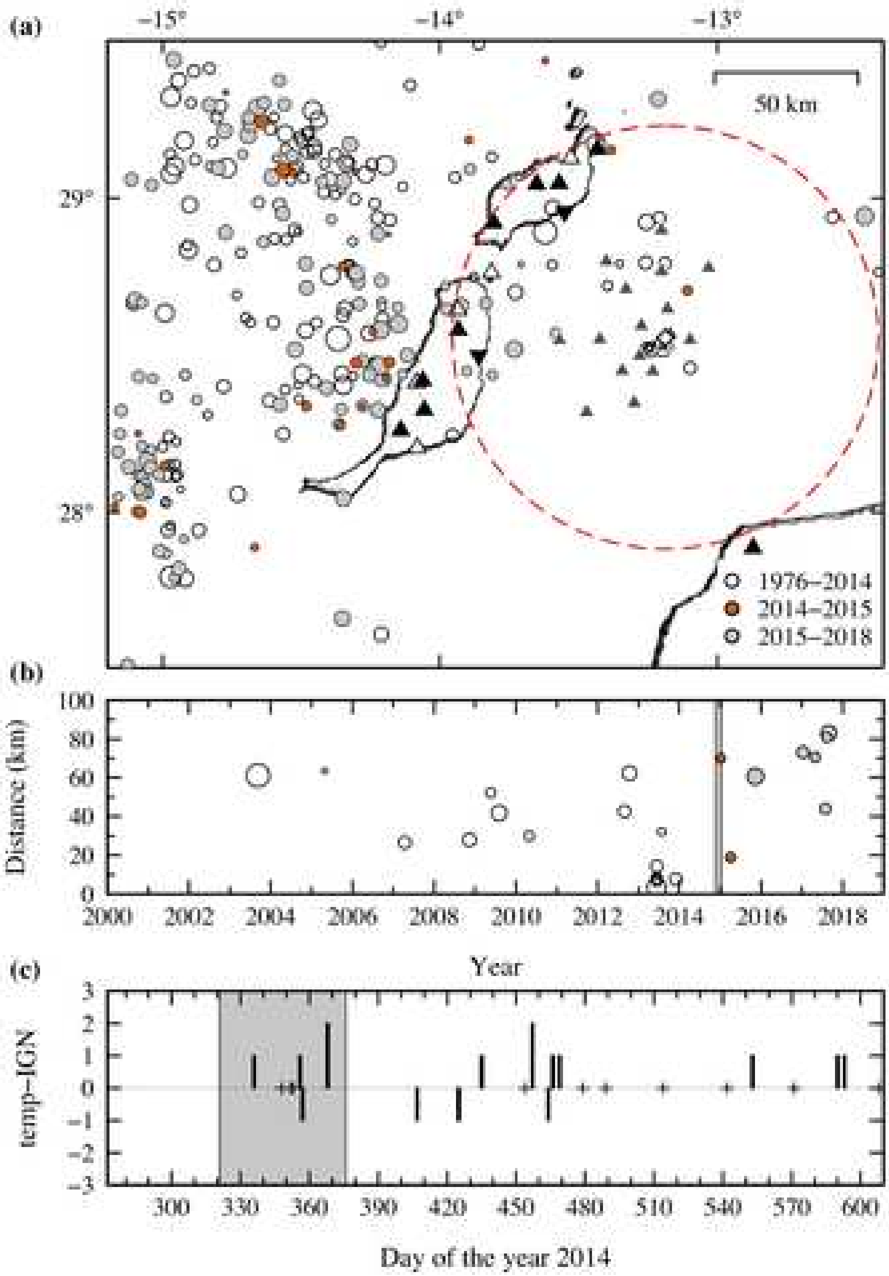

(a)
−15°
−14°
−13°
50 km
29°
28°
1976–2014
2014–2015
2015–2018
(b)
Distance (km)
Year
(c)
temp−IGN
Day of the year 2014

Figure 10

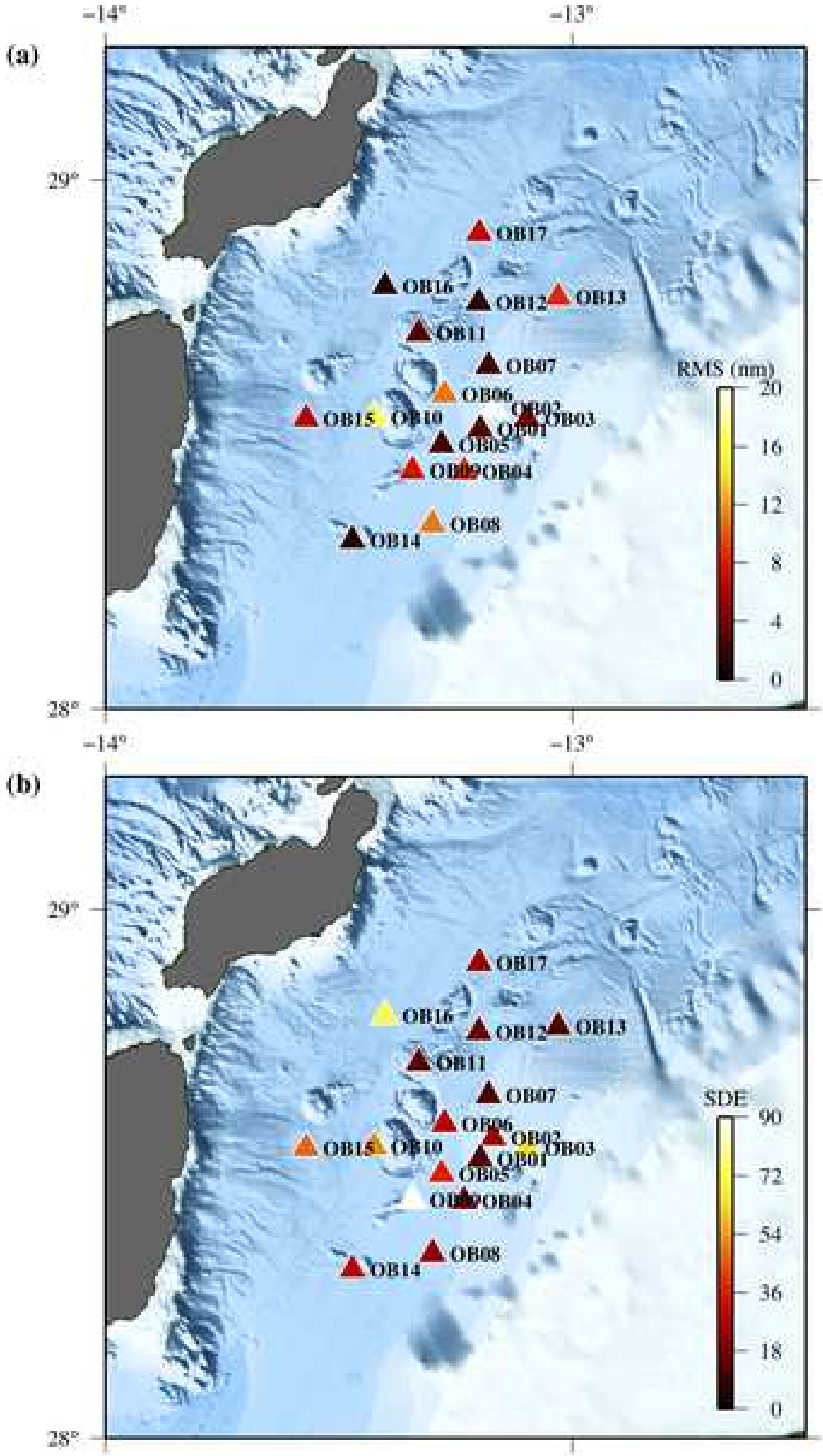
(a)
−14°
−13°
29°
28°
OB17
OB16
OB12
OB13
OB11
OB07
OB06
OB02
OB15
OB10
OB01
OB03
OB05
OB09
OB04
OB08
OB14
RMS (nm)
20
16
12
8
4
0
(b)
−14°
−13°
29°
28°
OB17
OB16
OB12
OB13
OB11
OB07
OB06
OB02
OB15
OB10
OB01
OB03
OB05
OB09
OB04
OB08
OB14
SDE
90
72
54
36
18
0